S. Moeini-Ardakani, M.T. Kamali and H.M. Shodja\*

# Eccentric annular crack under general nonuniform internal pressure

DOI 10.1515/jmbm-2016-0007

**Abstract:** For a better approximation of ring-shaped and toroidal cracks, a new eccentric annular crack model is proposed and an analytical approach for determination of the corresponding stress intensity factors is given. The crack is subjected to arbitrary mode I loading. A rigorous solution is provided by mapping the eccentric annular crack to a concentric annular crack. The analysis leads to two decoupled Fredholm integral equations of the second kind. For the sake of verification, the problem of a conventional annular crack is examined. Furthermore, for various crack configurations of an eccentric annular crack under uniform tension, the stress intensity factors pertaining to the inner and outer crack edges are delineated in dimensionless plots.

**Keywords:** annular crack; integral equations; three-part mixed boundary value problem.

#### 1 Introduction

An annular crack consists of two concentric circular edges that are coplanar; such a crack is the simplest idealization of a toroidal crack, which is frequently observed at material interfaces or in homogeneous media after fabrication. For this reason, many researchers considered an annular crack inside isotropic materials under uniform far-field loading by employing the asymptotic and approximate methods used by Smetanin [1], Moss and Kobayashi [2], and Shibuya et al. [3]. Perhaps, the most significant attempt that has been made in this area belongs to Fabrikant [4],

a pair of non-singular Fredholm integral equations of the second kind. Saxena and Dhaliwal [5] examined the problem of an annular crack surrounding an elastic fiber in a transversely isotropic matrix. They reduced the mixedboundary value problem to a singular integral equation. Shindo et al. [6] considered the problem of a permeable annular crack in a piezoelectric fiber enclosed by an infinite isotropic solid subjected to mode I far-field loading. Their formulation lead to a pair of coupled singular integral equations. Recently, Shodja et al. [7] considered a concentric set of energetically consistent annular and penny-shaped cracks in an infinite, transversely isotropic piezoelectric medium under a uniform far-field electromechanical loading parallel to the poled direction and perpendicular to the crack faces. They reduced the problem to a Fredholm integral equation of the second kind. A more realistic idealization of a toroidal crack encoun-

who reduced the problem of a mode I annular crack with non-axisymmteric loading over the faces of the crack to

tered in materials is inferred by considering the angular dependence of crack size, that is the inner and outer crack edges, generally, consist of two eccentric circles. It is proposed to give an accurate analytical solution for such an eccentric annular crack within an isotropic infinite body under nonuniform (non-axisymmetric) internal pressure. The solution of the problem is expressed in the form of a set of two decoupled Fredholm integral equations of the second kind. Subsequently, by employing a numerical scheme suggested by Atkinson [8], the algorithm for the solution of these equations is provided. The solution of the eccentric annular crack under uniform mode I loading is readily obtained as a limiting case and presented in this work. Furthermore, the stress intensity factors are delineated in dimensionless plots for different values corresponding to (1) ratio of the inner to the outer radius and (2) ratio of the eccentricity to inner or outer radius.

## 2 Governing equations and statement of the problem

The equilibrium equations in the absence of body forces can be expressed as

<sup>\*</sup>Corresponding author: H.M. Shodja, Department of Civil Engineering, Sharif University of Technology, Tehran 11155-9313, Iran, Tel.: +98 21 66164209, Fax: +98 21 66072555, e-mail: shodja@sharif.edu; and Institute for Nanoscience and Nanotechnology, Sharif University of Technology, Tehran 11155-9313, Iran

**S. Moeini-Ardakani:** Department of Civil and Environmental Engineering, Massachusetts Institute of Technology, Cambridge, MA 02139, USA

M.T. Kamali: Department of Civil Engineering, University of Hormozgan, Bandar Abbas 3995, Iran

$$\nabla . \sigma = 0, \tag{1}$$

where  $\sigma$  denotes the stress tensor. The corresponding constitutive relations for isotropic materials may be written as follows:

$$\boldsymbol{\sigma} = \mu \left\{ \nabla \mathbf{u} + (\nabla \mathbf{u})^{\mathrm{T}} + \frac{2\nu}{1 - 2\nu} (\nabla \cdot \mathbf{u}) \mathbf{I} \right\}, \tag{2}$$

where **u** is the displacement vector; **I**, the identity matrix;  $\mu$ , the shear modulus; and  $\nu$ , the Poisson's ratio.

Consider an eccentric annular crack with eccentricity e embodied by an isotropic matrix. Let  $r_1$  and  $r_2$  denote the inner and the outer radii of the crack edges, respectively. The origin of the Cartesian coordinate system  $O(x_1, x_2, x_3)$  is set in such a way that the crack lies in the  $x_1x_2$ -plane and the center of the inner circle is located at  $(c_1, 0, 0)$ , where

$$c_1 = \frac{\sqrt{1 + 4r_1^2 a^2} - 1}{2a},\tag{3}$$

and a is a constant depending on  $r_1$ ,  $r_2$  and e which will be introduced shortly. The faces of the crack are subjected to an arbitrary pressure,  $p(x_1, x_2)$ , as elucidated in Figure 1.

Suppose that the crack plane lies in  $\mathbb{R}^2$ , coinciding with the  $x_1x_2$ -plane. Let  $\mathbb{D}_1$  be the domain bounded by the inner crack edge, and  $\mathbb{D}_2$ , the complement of the domain enclosed by the outer crack edge. It can easily be understood that the crack occupies the region  $\mathbb{R}^2$ - $(\mathbb{D}_1 \cup \mathbb{D}_2)$  in the  $x_1x_2$ -plane, where

$$\mathbb{D}_1 = \{ (x_1, x_2) \in \mathbb{R}^2 | (x_1 - c_1)^2 + x_2^2 < r_1^2 \}, \tag{4}$$

$$\mathbb{D}_{2} = \{(x_{1}, x_{2}) \in \mathbb{R}^{2} | (x_{1} - c_{1} - e)^{2} + x_{2}^{2} > r_{2}^{2} \}.$$
 (5)

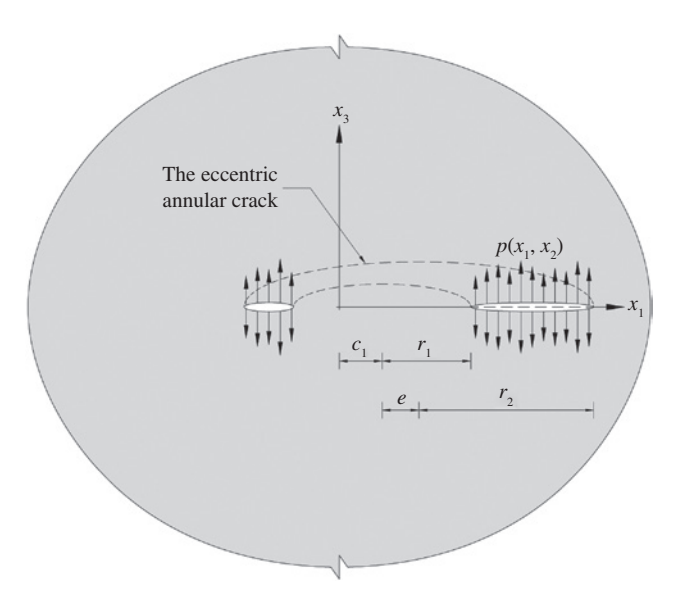


Figure 1: The geometry of the eccentric annular crack.

Due to symmetry of the problem with respect to  $x_3$ =0, the mixed-boundary conditions may be written as

$$u_3(x_1, x_2, 0)=0 \quad (x_1, x_2) \in \mathbb{D}_1,$$
 (6)

$$\sigma_{33}(x_1, x_2, 0) = -p(x_1, x_2) \quad (x_1, x_2) \in \mathbb{R}^2 - (\mathbb{D}_1 \cup \mathbb{D}_2),$$
 (7)

$$u_3(x_1, x_2, 0)=0 \quad (x_1, x_2) \in \mathbb{D}_2,$$
 (8)

$$\sigma_{13}(x_1, x_2, 0) = 0 \quad (x_1, x_2) \in \mathbb{R}^2,$$
 (9)

$$\sigma_{23}(x_1, x_2, 0) = 0 \quad (x_1, x_2) \in \mathbb{R}^2,$$
 (10)

where  $u_i$  and  $\sigma_{ij}$  (i, j=1, 2, 3) denote the components of displacement and stress fields, respectively.

### 3 The Papkovich-Neuber solution and three-dimensional mapping

In order to solve the mixed boundary value problem stated in Section 2, the well-known Papkovich-Neuber potential function is employed:

$$2\mu \mathbf{u} = 4(1-\nu)\psi - \nabla(\mathbf{x}.\psi + \varphi), \tag{11}$$

where  $\psi$  and  $\varphi$  are the harmonic functions with respect to  $(x_1, x_2, x_3)$ . One can conventionally take

$$\psi_1 = \psi_2 \equiv 0, \quad \psi_3 = \frac{1}{1 - 2\nu} \frac{\partial \varphi}{\partial x_3}.$$
 (12)

In view of Eqs. (11), (2) and (6)–(8), it can be shown that

$$\psi_3 = 0, (x_1, x_2) \in \mathbb{D}_1,$$
 (13)

$$\frac{\partial \psi_3}{\partial x_3} = -p(x_1, x_2), \quad (x_1, x_2) \in \mathbb{R}^2 - (\mathbb{D}_1 \cup \mathbb{D}_2), \tag{14}$$

$$\psi_3 = 0, (x_1, x_2) \in \mathbb{D}_2$$
 (15)

on  $x_3$ =0. Thus, the original problem has been reduced to a three-part mixed boundary value problem for  $\psi_3$ . The eccentricity of the annular crack has lead to the above conditions, which are difficult to work with. Therefore, a three-dimensional mapping similar to that of the two-dimensional case introduced by Muskhelishvili [9] is defined, which transforms the set of eccentric circles to a set of concentric circles, as follows:

$$\zeta = \frac{z}{1+az}, \quad z = \frac{\zeta}{1-a\zeta}, \quad \zeta = \xi_1 + i\xi_2, \quad z = x_1 + ix_2,$$
 (16)

$$\xi_3 = \frac{x_3}{(ax_1+1)^2 + a^2x_2^2}, \quad a = \frac{e}{\sqrt{(r_1^2 - r_2^2)^2 - 2e^2(r_1^2 + r_2^2) + e^4}}.$$
 (17)

These relations are expressible in a compact form as

$$\xi_i = \frac{x_i + \delta_{i1} a(x_1^2 + x_2^2)}{(ax_1 + 1)^2 + a^2 x_2^2}, \quad i = 1, 2, 3,$$
 (18)

where  $\delta_{ij}$  (i, j=1, 2, 3) denotes the Kronecker delta. The details of the mapping are shown in Figure 2.

As is shown in the Appendix, in the transformed space,  $\psi_3$  is a harmonic function:

$$\left(\frac{\partial^2}{\partial \xi_1^2} + \frac{\partial^2}{\partial \xi_2^2} + \frac{\partial^2}{\partial \xi_3^2}\right) \psi_3 = 0.$$
 (19)

A cylindrical coordinate system  $(\rho, \phi, \xi_3)$  is defined in the transformed space. Therefore, boundary conditions (13)–(15) are transformed to

$$\psi_3 = 0, \ \rho < \rho_1,$$
 (20)

$$\frac{\partial \psi_3}{\partial \xi_2} = \frac{-p(\rho, \phi)}{1 + a^2 \rho^2 - 2a\rho \cos \phi}, \quad \rho_1 < \rho < \rho_2, \tag{21}$$

$$\psi_3 = 0, \ \rho_2 < \rho$$
 (22)

on  $\xi_3$ =0 and 0< $\phi$ <2 $\pi$ , where  $\rho_1$  and  $\rho_2$  are the respective radii of the inner and outer crack-tips in the transformed space,

$$\rho_i = \frac{\sqrt{1 + 4r_i^2 a^2} - 1}{2r_i a^2}, \quad i = 1, 2.$$
 (23)

At this point, by the well-known method proposed by Fabrikant [4], the three-part mixed boundary value problem defined by (20)–(22) reduces to

$$F_{\pm}(\rho,\phi) \pm \int_{0}^{2\pi} \int_{0}^{\sqrt{\rho_{1}/\rho_{2}}} k(\rho\rho_{0},\phi-\phi_{0}) F_{\pm}(\rho_{0},\phi_{0}) d\rho_{0} d\phi_{0} = G_{\pm}(\rho,\phi),$$

$$0 < \rho < \sqrt{\frac{\rho_{1}}{\rho_{2}}},$$
(24)

with

$$G_{+}(\rho,\phi) = g_{1}(\sqrt{\rho_{1}\rho_{2}}\rho,\phi) \pm g_{2}(\sqrt{\rho_{1}\rho_{2}}/\rho,\phi)/\rho, \tag{25}$$

$$k(\rho, \phi) = \frac{1}{\pi^2} \left\{ 2 \operatorname{Re} \left[ \frac{1}{\overline{\gamma} \sqrt{\rho \gamma \overline{\gamma}}} \tan^{-1} \sqrt{\frac{\rho \gamma}{\overline{\gamma}}} \right] + \frac{1}{\rho \gamma \overline{\gamma}} \right\}, \tag{26}$$

where  $\overline{\gamma}$  is the complex conjugate of  $\gamma$ :

$$\gamma = \frac{e^{i\varphi} \cdot \rho}{\sqrt{e^{i\varphi}} \rho},\tag{27}$$

$$g_{1}(\rho, \phi) = \int_{0}^{2\pi} \int_{\rho_{1}}^{\rho_{2}} \frac{\rho_{0}\sqrt{\rho_{0}^{2} - \rho^{2}} p(\rho_{0}, \phi_{0}) d\rho_{0} d\phi_{0}}{2\pi [\rho^{2} + \rho_{0}^{2} - 2\rho\rho_{0}\cos(\phi - \phi_{0})][1 + a^{2}\rho_{0}^{2} - 2a\rho_{0}\cos\phi_{0}]}, (28)$$

$$g_{2}(\rho,\phi) = \int_{0}^{2\pi} \int_{\rho_{1}}^{\rho_{2}} \frac{\rho_{0}\sqrt{\rho^{2} - \rho_{0}^{2}} p(\rho_{0},\phi_{0}) d\rho_{0} d\phi_{0}}{2\pi [\rho^{2} + \rho_{0}^{2} - 2\rho\rho_{0}\cos(\phi - \phi_{0})][1 + a^{2}\rho_{0}^{2} - 2a\rho_{0}\cos\phi_{0}]}.$$
(29)

 $F_+(\rho,\phi)$  and  $F_-(\rho,\phi)$  can be interpreted through the following equations:

$$\frac{F_{+}(\rho/\sqrt{\rho_{1}\rho_{2}},\phi)+F_{-}(\rho/\sqrt{\rho_{1}\rho_{2}},\phi)}{2} = \int_{\rho}^{\rho_{1}} \frac{\rho_{0} d\rho_{0}}{\sqrt{\rho_{0}^{2} \cdot \rho^{2}}} \mathcal{L}\left(\frac{\rho}{\rho_{0}}\right) \frac{\partial \psi_{3}}{\partial \xi_{3}}(\rho_{0},\phi,0), \quad \rho < \rho_{1}, \tag{30}$$

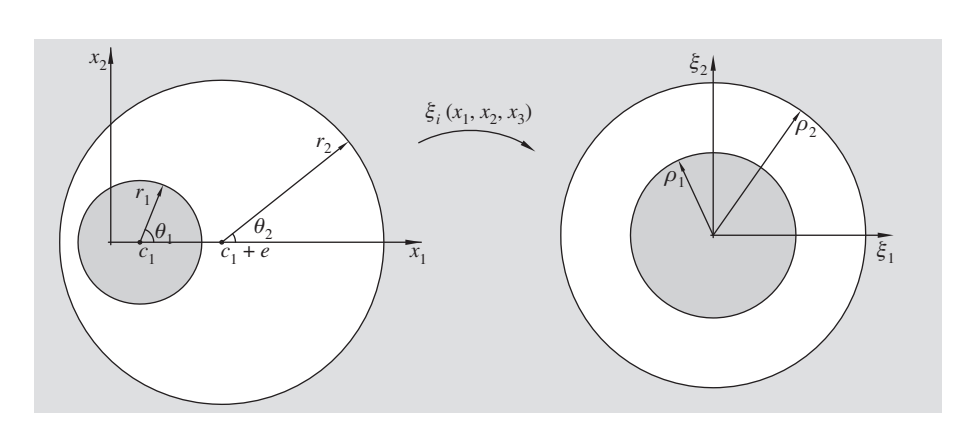


Figure 2: Top view of the three-dimensional mapping given by Eq. (18).

$$\frac{F_{+}(\sqrt{\rho_{1}\rho_{2}}/\rho,\phi)\cdot F(\sqrt{\rho_{1}\rho_{2}}/\rho,\phi)}{2\rho/\sqrt{\rho_{1}\rho_{2}}} = \int_{\rho_{2}}^{\rho} \frac{\rho_{0}d\rho_{0}}{\sqrt{\rho^{2}\cdot\rho_{2}^{2}}} \mathcal{L}\left(\frac{\rho_{0}}{\rho}\right) \frac{\partial\psi_{3}}{\partial\xi_{3}}(\rho_{0},\phi,0), \quad \rho_{2}<\rho, \tag{31}$$

or

$$\frac{\partial \psi_{3}}{\partial \xi_{3}} = \frac{2}{\pi \rho} \mathcal{L}(\rho) \frac{\mathrm{d}}{\mathrm{d}\rho} \int_{\rho}^{\rho_{1}} \frac{\rho_{0} \mathrm{d}\rho_{0}}{\sqrt{\rho_{0}^{2} - \rho^{2}}} \mathcal{L}\left(\frac{1}{\rho_{0}}\right) \frac{F_{+}(\rho_{0}/\sqrt{\rho_{1}\rho_{2}}, \phi) + F_{-}(\rho_{0}/\sqrt{\rho_{1}\rho_{2}}, \phi)}{2}, \quad \rho < \rho_{1}, \tag{32}$$

$$\frac{\partial \psi_{3}}{\partial \xi_{3}} = \frac{2}{\pi \rho} \mathcal{L} \left( \frac{1}{\rho} \right) \frac{\mathrm{d}}{\mathrm{d}\rho} \int_{\rho_{2}}^{\rho} \frac{\rho_{0} \mathrm{d}\rho_{0}}{\sqrt{\rho^{2} - \rho_{0}^{2}}} \mathcal{L}(\rho_{0})$$

$$\frac{F_{+}(\sqrt{\rho_{1}\rho_{2}}/\rho_{0}, \phi) - F_{-}(\sqrt{\rho_{1}\rho_{2}}/\rho_{0}, \phi)}{2\rho_{0}/\sqrt{\rho_{1}\rho_{2}}}, \rho_{2} < \rho \tag{33}$$

on  $\xi_3$ =0, and  $\mathcal{L}$  is an integral operator defined as

$$\mathcal{L}(k)f(\rho,\phi) = \frac{1}{2\pi} \int_0^{2\pi} \frac{(1-k^2)f(\rho,\phi_0)d\phi_0}{1+k^2-2k\cos(\phi-\phi_0)}.$$
 (34)

If  $(r_1, \theta_1)$  and  $(r_2, \theta_2)$  denote the polar coordinates with origins at the center of the inner and outer crack edges in the untransformed space, then the stress intensity factors can be written as

$$K_{I}^{(2)}(\theta_{2}) = \frac{\sqrt{1 + a^{2} \rho_{2}^{2} - 2a \rho_{2} \cos \phi_{2}}}{\sqrt{\pi \rho_{2}} / \sqrt{\rho_{1}}} [F_{+}(\sqrt{\rho_{1}/\rho_{2}}, \phi_{2}) - F_{-}(\sqrt{\rho_{1}/\rho_{2}}, \phi_{2})],$$
(38)

where

$$\phi_i = 2\cot^{-1}\left(\frac{1+a\rho_i}{1-a\rho_i}\right)\cot\frac{\theta_i}{2}, \quad 0<\theta_i<2\pi, \quad i=1, 2.$$
 (39)

For the sake of completeness, a brief discussion on the numerical methodology for the two-dimensional Fredholm integral equations (24) is given in the remainder of this section.

By virtue of the numerical method introduced by Atkinson [8], the governing Fredholm integral equations can be converted to a set of linear algebraic equations. The intervals  $[0, \sqrt{\rho_1/\rho_2}]$  and  $[0, 2\pi]$  are divided into  $N_1$  and  $N_2$  equal segments, respectively, so that

$$\lambda_{i} = \frac{2i-1}{2N_{1}} \sqrt{\frac{\rho_{1}}{\rho_{2}}}, \quad \omega_{j} = \frac{2j-1}{2N_{2}} 2\pi \quad i=1, 2, \dots, N_{1}, \quad j=1, 2, \dots, N_{2}.$$
(40)

In view of these definitions, the unknown functions  $F_{+}(\lambda_{i},\omega_{i})$  are obtained from

$$[\mathbf{A}^{\pm}]\{\mathbf{B}^{\pm}\} = \{\mathbf{C}^{\pm}\},\tag{41}$$

where

$$\begin{cases}
A_{((i_{1}\cdot1)N_{2}+j_{1},(i_{2}\cdot1)N_{2}+j_{2})}^{\pm} = \delta_{i,i_{2}}\delta_{j_{i}j_{2}} \pm \frac{2\pi\sqrt{\frac{\rho_{1}}{\rho_{2}}}}{N_{1}N_{2}}k(\lambda_{i_{1}}\lambda_{i_{2}},\omega_{j_{1}}-\omega_{j_{2}}), \\
C_{(i_{1}\cdot1)N_{2}+j_{1}}^{\pm} = G_{\pm}(\lambda_{i_{1}},\omega_{j_{1}}), & i_{1}, i_{2}=1, 2, \cdots, N_{1}, \\
B_{(i_{2}\cdot1)N_{2}+j_{2}}^{\pm} = F_{\pm}(\lambda_{i_{2}},\omega_{j_{2}}), & j_{1}, j_{2}=1, 2, \cdots, N_{2}.
\end{cases}$$
(42)

(37)

$$K_I^{(1)}(\theta_1) = \lim_{r \to r'} \sqrt{2\pi(r_1 - r)} \sigma_{33}(c_1 + r\cos\theta_1, r\sin\theta_1),$$
 (35)

$$K_{I}^{(2)}(\theta_{2}) = \lim_{r \to r_{2}^{+}} \sqrt{2\pi(r-r_{2})} \sigma_{33}(c_{1} + e + r\cos\theta_{2}, r\sin\theta_{2}),$$
 (36)

where superscripts 1 and 2 pertain to the inner and outer borders of the crack, respectively. Alternatively,

$$K_I^{(1)}(\theta_1) = \frac{\sqrt{1 + a^2 \rho_1^2 - 2a\rho_1 \cos\phi_1}}{\sqrt{\pi\rho_1}} [F_+(\sqrt{\rho_1/\rho_2}, \phi_1) + F_-(\sqrt{\rho_1/\rho_2}, \phi_1)],$$

4 Results and discussion

At first, for the sake of verification, two problems of a concentric annular crack subjected to uniform (Section 4.1) and non-axisymmetric (Section 4.2) internal pressures that are available in the literature are readily re-examined as the special cases of the current work. Subsequently, the problem of an eccentric annular crack under uniform far-field tension is addressed in Section 4.3.

<b>Table 1:</b> Comparison of the values of the inner and outer stress intensity factors for various ratios of $c/r_c$ for the case of a concentric annular
crack with those of Noda et al. [11] and Tada et al. [10].

c/r <sub>c</sub>	$K_{l}^{(1)}/(\sigma_{o}\sqrt{\pi c})$			$K_{I}^{(2)}/(\sigma_{0}\sqrt{\pi c})$		
	Current study	Ref. [11]	Ref. [10]	Current study	Ref. [11]	Ref. [10]
0.1	1.030	1.030	1.031	0.979	0.979	0.979
0.2	1.068	1.068	1.069	0.963	0.963	0.963
0.3	1.118	1.118	1.117	0.950	0.950	0.950
0.4	1.182	1.182	1.180	0.939	0.939	0.939
0.5	1.269	1.269	1.265	0.930	0.930	0.930
0.6	1.390	1.390	1.385	0.922	0.922	0.922
0.7	1.572	1.573	1.567	0.916	0.916	0.915
0.8	1.887	1.885	1.881	0.910	0.910	0.910
0.9	2.616	2.577	2.610	0.905	0.903	0.904

#### 4.1 Concentric annular crack under uniform tension

The numerical values of the stress intensity factors pertinent to the concentric annular crack under uniform tension are available in the Handbook by Tada et al. [10] as well as in the work of Noda et al. [11]. As it is evident from Table 1, the numerical values of the normalized stress intensity factors  $K_I^{(1)}/(\sigma_0\sqrt{\pi c})$  and  $K_I^{(2)}/(\sigma_0\sqrt{\pi c})$ reproduced for different ratios of  $c/r_c$  via the present theory with zero eccentricity (e=0) are in good agreement with their results; note that  $c=(r_1-r_1)/2$  and  $r_{\rm e}=(r_{\rm e}+r_{\rm e})/2$ . Furthermore, the stress intensity factors for the special cases of center crack and penny-shaped crack can readily be calculated in the limits as  $r_1/r_2 \rightarrow 1(c/r_2 \rightarrow 0)$ and  $r_1/r_2 \rightarrow 0$  ( $c/r_c \rightarrow 1$ ), respectively. For the center crack, the current theory yields  $K_I^{(1)}/(\sigma_0\sqrt{\pi c})=1.004$  and  $K_{L}^{(2)}/(\sigma_{0}\sqrt{\pi c})=1.002$ , which are in reasonable agreement with the exact values of 1. For the case of the penny-shaped crack, the current theory results in  $K_L^{(2)}/(\sigma_0\sqrt{\pi c})=0.901$  as compared to the exact value of  $2\sqrt{2/\pi} \sim 0.900$ .

Figure 3A and B compare, respectively, the variations of the normalized stress intensity factors  $K_{i}^{(i)}/(\sigma_{0}\sqrt{\pi c})$ , i=1, 2 in terms of  $r_{i}/r_{0}$  obtained using the current theory with those from the Handbook by Tada et al. [10]. The results are in good agreement, and moreover, for the above-mentioned limiting cases of a center crack  $(r_1/r_2\rightarrow 1)$  and a penny-shaped crack  $(r_1/r_2\rightarrow 0)$ , the results converge to the exact values of 1 [both  $K_I^{(1)}/(\sigma_0 \sqrt{\pi c})$  and  $K_t^{(2)}/(\sigma_0\sqrt{\pi c})$ ] and  $2\sqrt{2}/\pi(K_t^{(2)}/(\sigma_0\sqrt{\pi c}))$ , respectively. It is evident that the normalized stress intensity factor  $K_I^{(i)}/(\sigma_0\sqrt{\pi c})$  along the inner crack-tip (*i*=1) decreases with increasing  $r_1/r_2$ , while the trend for that of the outer crack-tip (i=2) is reversed.

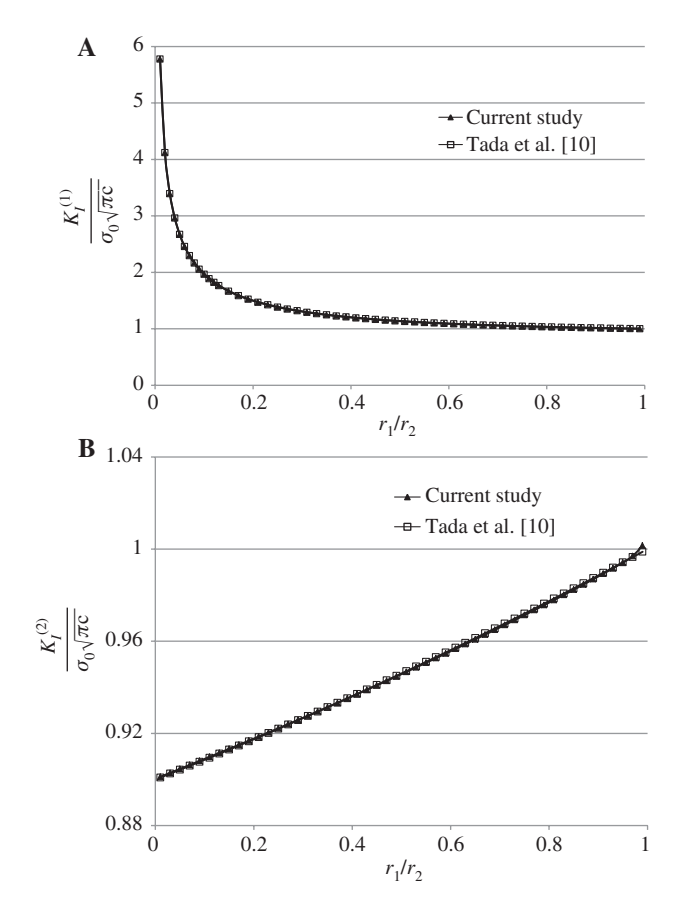


Figure 3: Comparison of the variations of the (A) inner and (B) outer stress intensity factors in terms of  $r_1/r_2$  for the case of concentric annular crack with those of Tada et al. [10].

#### 4.2 Concentric annular crack under non-axisymmetric loading

The represented solution is verified by examination of the reduced conventional concentric annular crack for which

e=0. For this special case,  $\rho_1$ = $r_1$  and  $\rho_2$ = $r_2$  and the right-hand side of (24) degenerates so that

$$g_{1}(\rho,\phi) = \int_{0}^{2\pi} \int_{\rho_{1}}^{\rho_{2}} \frac{\rho_{0} \sqrt{\rho_{0}^{2} - \rho^{2}} p(\rho_{0},\phi_{0}) d\rho_{0} d\phi_{0}}{2\pi [\rho^{2} + \rho_{0}^{2} - 2\rho\rho_{0} \cos(\phi - \phi_{0})]},$$
(43)

$$g_{2}(\rho,\phi) = \int_{0}^{2\pi} \int_{\rho_{1}}^{\rho_{2}} \frac{\rho_{0} \sqrt{\rho^{2} - \rho_{0}^{2}} p(\rho_{0},\phi_{0}) d\rho_{0} d\phi_{0}}{2\pi [\rho^{2} + \rho_{0}^{2} - 2\rho\rho_{0}\cos(\phi - \phi_{0})]}.$$
 (44)

It is seen that (43) and (44) are in complete agreement with the solution of an annular crack represented by Fabrikant [4].

### 4.3 Eccentric annular crack under uniform far-field tension

In Sections 2 and 3, the problem of an eccentric annular crack under arbitrary pressure over the faces of the crack was formulated in terms of two decoupled Fredholm integral equations. One of the most practical cases is the case of an eccentric annular crack under uniform far-field loading which is equivalent to uniform pressure over the crack faces; therefore, the stress intensity factors corresponding to this problem are examined for various crack configurations.

On setting  $p(x_1, x_2) = \sigma_0$ , the right-hand side of the Fredholm integral equations (24) degenerate, so that

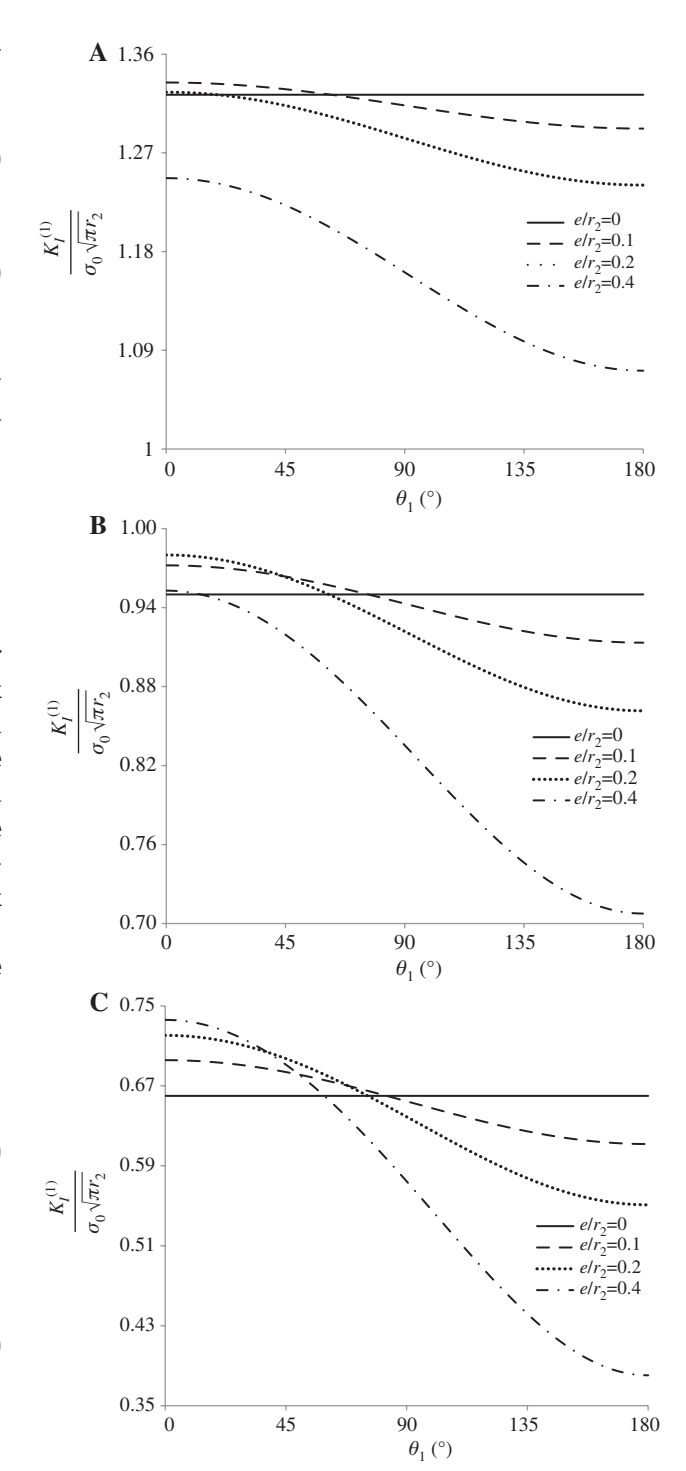
$$g_{1}(\rho,\phi) = \frac{-\mathbf{i}\sigma_{0}}{a^{2}\rho(z_{2}\overline{z}_{2})^{2}} \left[ z_{1} \tanh^{-1} \frac{\sqrt{1-\rho_{2}^{2}/\rho^{2}}}{z_{1}} - z_{1} \tanh^{-1} \frac{\sqrt{1-\rho_{1}^{2}/\rho^{2}}}{z_{1}} \right], \tag{45}$$

$$g_{2}(\rho, \phi) = \frac{-2\sigma_{0}}{\alpha^{2}\rho(z_{2}\overline{z}_{2})^{2}} \operatorname{Re} \left[ z_{2} \tanh^{-1} \frac{\sqrt{1-\rho_{2}^{2}/\rho^{2}}}{z_{2}} \right] - z_{2} \tanh^{-1} \frac{\sqrt{1-\rho_{1}^{2}/\rho^{2}}}{z_{2}} + \mathbf{i}g_{1}(\rho, \phi),$$
(46)

where

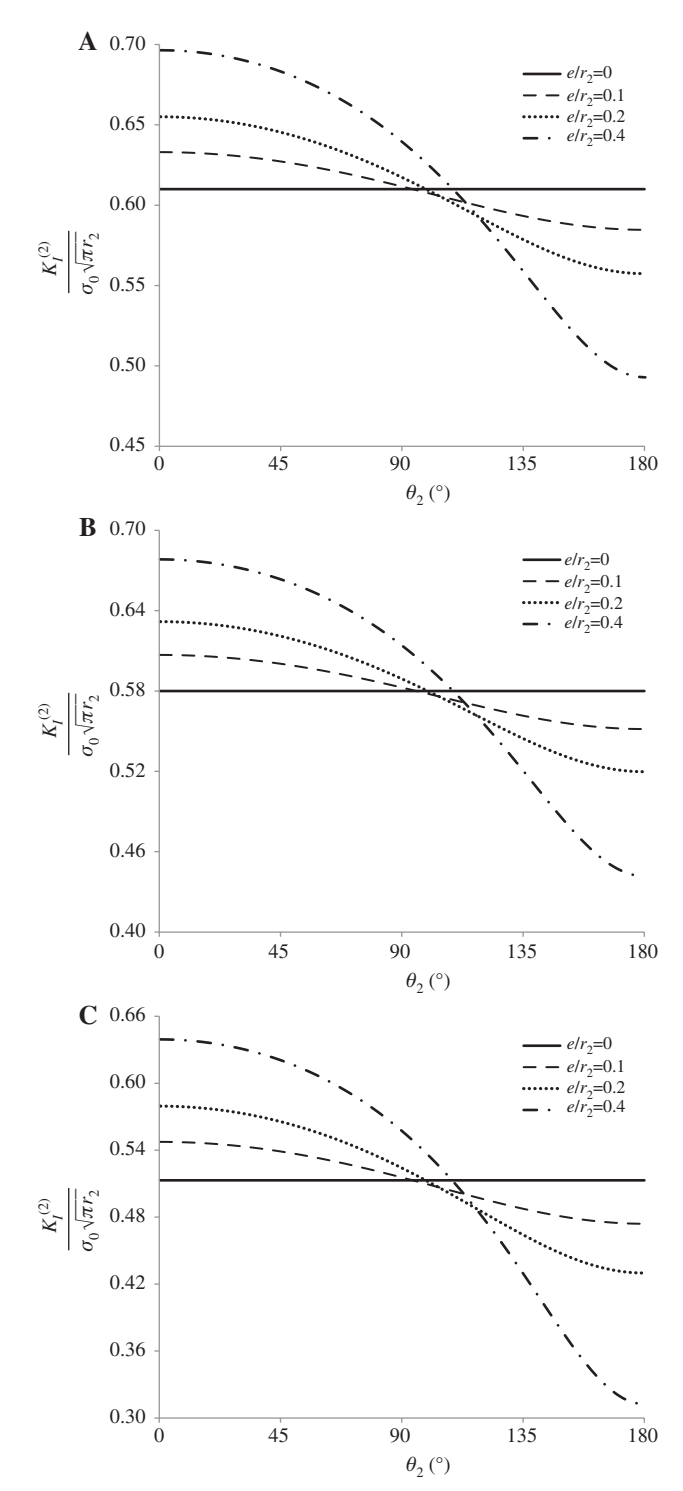
$$z_1 = \sqrt{1 - \frac{1}{a^2 \rho^2}}, z_2 = \sqrt{1 - \frac{e^{i\phi}}{a\rho}}.$$
 (47)

Figure 4A–C which correspond, respectively, to  $r_1/r_2$ =0.1, 0.2, 0.4 show the variation of the normalized stress intensity factor associated with the inner crack edge,  $K_I^{(1)}/(\sigma_0\sqrt{\pi r_2})$ , , with an angle  $\theta_1$ ; each figure displays four curves which are pertinent to  $e/r_2$ =0, 0.1, 0.2, 0.4. Similar sets of plots are provided for the outer crack edge in Figure 5A–C. It is observed that for all cases the stress



**Figure 4:** Effect of the eccentricity on the inner stress intensity factor for the cases: (A)  $r_1/r_2=0.1$ , (B)  $r_1/r_2=0.2$ , and (C)  $r_1/r_2=0.4$ .

intensity factors decrease with increasing  $r_1/r_2$ . For a given value of  $r_1/r_2$  and  $e/r_2$ , the stress intensity factor for the inner crack edge is larger than that of the outer crack edge. From comparison of the figures pertinent to the outer crack edge, it is seen that a curve for a given value  $e/r_2 \neq 0$  crosses



**Figure 5:** Effect of the eccentricity on the outer stress intensity factor for the cases: (A)  $r_1/r_2=0.1$ , (B)  $r_1/r_2=0.2$ , and (C)  $r_1/r_2=0.4$ .

the line  $e/r_2$ =0 at an angle  $\overline{\theta}_2$ , which remains unchanged as  $r_1/r_2$  varies. In other words for an annular crack with eccentricity,  $e/r_2 \neq 0$ , there exists an angle,  $0^{\circ} < \overline{\theta}_2 = \overline{\theta}_2 (e/r_2) < 180^{\circ}$  independent of the ratio  $r_1/r_2$  along the outer crack edge at which  $K_L^{(2)}/(\sigma_0\sqrt{\pi r_2})$  becomes equal to the stress intensity

factor pertinent to the outer crack edge of the concentric annular crack for which  $r_1$  and  $r_2$  are kept the same as those of the eccentric annular crack but  $e/r_2=0$ .

From Figure 4A–C, it is seen that for e>0 the maximum and minimum values of the stress intensity factor associated with the inner crack edge occur at  $\theta_1=0$  and  $\pi$ , respectively. Figure 5A–C reveal that similar observation holds for the outer crack edge.

Figure 6 shows the variation of the normalized value of the maximum stress intensity factor,  $K_I^{(1)}/(\sigma_0\sqrt{\pi r_2})$ , pertinent to the inner crack edge as a function of the normalized eccentricity,  $e/r_1$ , for different values of  $r_1/r_2$ =0.1, 0.2, 0.4. Similarly,  $K_I^{(2)}/(\sigma_0\sqrt{\pi r_2})$  versus  $e/r_1$  pertinent to the outer crack edge for  $r_1/r_2$ =0.1, 0.2, 0.4 has been plotted in Figure 7. From Figure 6, it is observed that

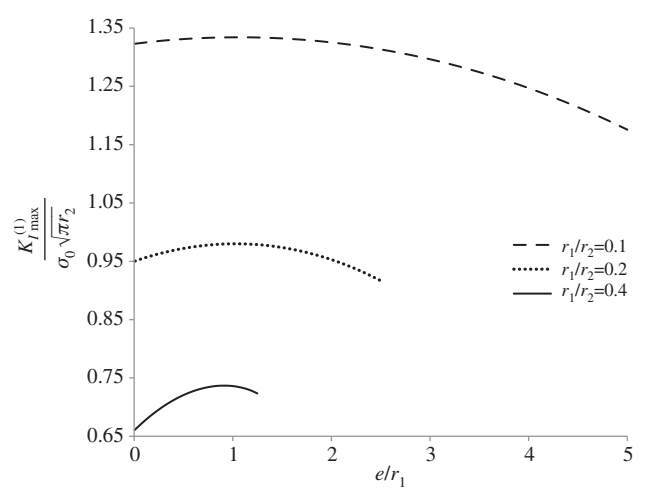


**Figure 6:** Variation of the maximum inner stress intensity factor in terms of eccentricity for the three cases of  $r_1/r_2$ =0.1, 0.2, and 0.4.

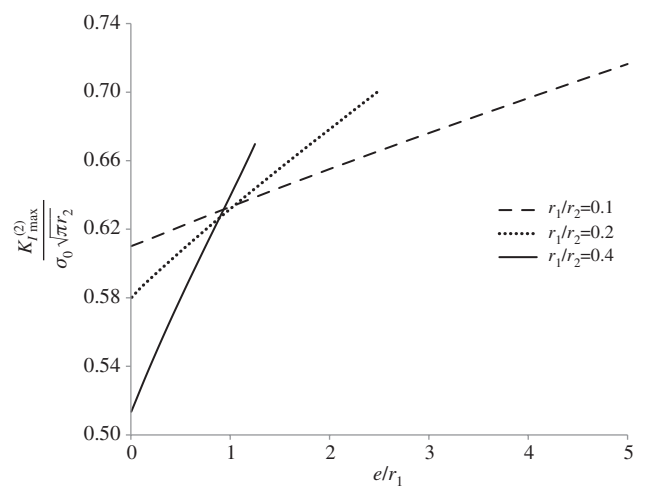


**Figure 7:** Variation of the maximum outer stress intensity factor in terms of eccentricity for the three cases of  $r_1/r_2=0.1$ , 0.2, and 0.4.

 $K_L^{(1)}/(\sigma_0\sqrt{\pi r_2})$  follows an increasing trend with the normalized eccentricity and reaches its peak value at about  $e/r_1 \approx 1$ .  $K_I^{(1)}/(\sigma_0 \sqrt{\pi r_2})$ , then decreases with further increase in  $e/r_1$ . However, Figure 7 shows that  $K_1^{(2)}/(\sigma_0\sqrt{\pi r_2})$ increases monotonically with  $e/r_1$ ; for larger values of  $r_1/r_2$ , there is a greater sensitivity to the change in the value of the normalized eccentricity,  $e/r_1$ .

#### **Appendix**

From Eq. (16), we have

$$\frac{\partial \psi_3}{\partial z} = \frac{\partial \psi_3}{\partial \xi} \frac{\partial \xi}{\partial z} + \frac{\partial \psi_3}{\partial \overline{\xi}} \frac{\partial \overline{\xi}}{\partial z} = \frac{1}{(1+az)^2} \frac{\partial \psi_3}{\partial \xi},$$
 (48)

$$\frac{\partial \psi_3}{\partial \overline{z}} = \frac{\partial \psi_3}{\partial \zeta} \frac{\partial \zeta}{\partial \overline{z}} + \frac{\partial \psi_3}{\partial \overline{\zeta}} \frac{\partial \overline{\zeta}}{\partial \overline{z}} = \frac{1}{(1 + a\overline{z})^2} \frac{\partial \psi_3}{\partial \overline{\zeta}}.$$
 (49)

Using the above equations, we can write

$$\frac{\partial^{2} \psi_{3}}{\partial z \partial \overline{z}} = \frac{1}{(1+az)^{2}} \frac{\partial}{\partial \xi} \left[ \frac{1}{(1+a\overline{z})^{2}} \frac{\partial \psi_{3}}{\partial \overline{\xi}} \right] = \frac{1}{(1+az)^{2}} \frac{\partial}{\partial \xi} \left[ (1-a\overline{\xi})^{2} \frac{\partial \psi_{3}}{\partial \overline{\xi}} \right] \\
= \frac{(1-a\overline{\xi})^{2}}{(1+az)^{2}} \frac{\partial^{2} \psi_{3}}{\partial \xi \partial \overline{\xi}} = \frac{1}{(1+az)^{2}(1+a\overline{z})^{2}} \frac{\partial^{2} \psi_{3}}{\partial \xi \partial \overline{\xi}} = \frac{1}{|(1+az)|^{4}} \frac{\partial^{2} \psi_{3}}{\partial \xi \partial \overline{\xi}},$$
(50)

which can be combined with the following equations:

$$4\frac{\partial^2 \psi_3}{\partial z \partial \overline{z}} = \frac{\partial^2 \psi_3}{\partial x_1^2} + \frac{\partial^2 \psi_3}{\partial x_2^2},\tag{51}$$

$$4\frac{\partial^2 \psi_3}{\partial \xi \partial \overline{\xi}} = \frac{\partial^2 \psi_3}{\partial \xi_2^2} + \frac{\partial^2 \psi_3}{\partial \xi_2^2}$$
 (52)

to give

$$\frac{\partial^2 \psi_3}{\partial x_1^2} + \frac{\partial^2 \psi_3}{\partial x_2^2} = \frac{1}{|(1+az)|^4} \left( \frac{\partial^2 \psi_3}{\partial \xi_1^2} + \frac{\partial^2 \psi_3}{\partial \xi_2^2} \right). \tag{53}$$

Moreover, from Eq. (18) we have

$$\frac{\partial \psi_{3}}{\partial x_{3}} = \frac{\partial \psi_{3}}{\partial \xi_{1}} \frac{\partial \xi_{1}}{\partial x_{3}} + \frac{\partial \psi_{3}}{\partial \xi_{2}} \frac{\partial \xi_{2}}{\partial x_{3}} + \frac{\partial \psi_{3}}{\partial \xi_{3}} \frac{\partial \xi_{3}}{\partial x_{3}} = \frac{1}{(ax_{1}+1)^{2} + a^{2}x_{2}^{2}} \frac{\partial \psi_{3}}{\partial \xi_{3}}$$

$$= \frac{1}{|(1+az)|^{2}} \frac{\partial \psi_{3}}{\partial \xi_{3}}, \tag{54}$$

and similarly,

$$\frac{\partial^2 \psi_3}{\partial x_3^2} = \frac{1}{|(1+az)|^4} \frac{\partial^2 \psi_3}{\partial \xi_3^2}.$$
 (55)

Therefore, we have

$$\frac{\partial^2 \psi_3}{\partial \xi_1^2} + \frac{\partial^2 \psi_3}{\partial \xi_2^2} + \frac{\partial^2 \psi_3}{\partial \xi_3^2} = \frac{1}{|(1+az)|^4} \left( \frac{\partial^2 \psi_3}{\partial x_1^2} + \frac{\partial^2 \psi_3}{\partial x_2^2} + \frac{\partial^2 \psi_3}{\partial x_3^2} \right). \tag{56}$$

This relation shows that if a function is harmonic with respect to the  $(x_1, x_2, x_3)$  coordinates, it will also be harmonic with respect to the transformed coordinates  $(\xi_1, \xi_2, \xi_3).$ 

#### References

- [1] Smetanin Bl. Prikl. Math. Mekh. 1967, 32, 461-466.
- [2] Moss LW, Kobayashi AS. Int. J. Fract. Mech. 1971, 7, 89-99.
- [3] Shibuya T, Nakahara I, Koizumi T. J. Appl. Math. Mech. (ZAMM) 1975, 55, 395-402.
- [4] Fabrikant VI. Mixed Boundary Value Problems of Potential Theory and their Applications in Engineering, Kluwer Academic Publishers: Dordrecht, 1991.
- [5] Saxena HS, Dhaliwal RS. Engng. Fract. Mech. 1993, 44, 963–969.
- [6] Shindo Y, Lin S, Narita F. J. Engng. Math. 2007, 59, 83-97.
- Shodja HM, Moeini-Ardakani SS, Eskandari M. ASME J. Appl. Mech. 2011, 78, 021010.
- [8] Atkinson K. SIAM J. Numer. Anal. 1976, 4 (3), 337-348.
- Muskhelishvili NI. Some Basic Problems of the Mathematical Theory of Elasticity, P. Noordhoff Ltd: Groningen Holland, 1953.
- Tada H, Paris PC, Irwin GR. The Stress Analysis of Cracks Handbook, ASME Press: New York, 2000.
- Noda N-A, Kagita M, Chen MC, Oda K. Int. J. Solids Struct. 2003, 40,6577-6592.